Improvements of Time-Domain Transmission Waveform and Eye Diagram of Serpentine Delay Line Using Open-Stub Type Guard Traces in Embedded Microstrip Line

Guang-Hwa Shiue, *Member, IEEE*, Jia-Hung Shiu, Po-Wei Chiu, and Che-Ming Hsu

***Abstract*—The utilization of guard traces with two grounded vias at both ends to improve the time-domain transmission (TDT) waveform and eye diagram for a serpentine delay line has been investigated. However, it is not easy to accomplish because the position of the pad of a grounded via is surrounded by a serpentine trace. This is especially true for normal manufacturing technology, where the size of via pad is larger. Therefore, this paper proposes the use of open-stub type guard traces (OSGTs), to reduce crosstalk noise in the TDT waveform and eye diagram of a serpentine delay line, in an embedded microstrip structure. The OSGT, i.e., the guard trace, at one end is a grounded via and at the other is open-ended. The crosstalk reduced efficiency for using OSGTs is almost the same as when using two-grounded-via type guard traces on the serpentine delay line in the time-domain. This is because, the open-end of the OSGTs leads to the noise cancellation mechanism. A graphic method was used to illustrate the noise cancellation mechanism and ringing crosstalk noise generation on the TDT waveform. Two useful design graphs were used to evaluate the maximum flat voltage level of a laddering wave. Based on HSPICE simulation, it was demonstrated that the utilization of OSGTs can significantly reduce the original TDT crosstalk level, thereby greatly improving eye opening and jitter. Finally, this paper also performs time-domain measurement and 3-D full-wave simulation to validate the proposed analyzes.**

***Index Terms*—Eye diagram, guard traces, open-stub type guard trace, serpentine delay line, signal integrity, time-domain transmission, two-grounded-via type.**

I. INTRODUCTION

AS THE cycle time of a computer system enters the sub-nanosecond region, the fraction of the cycle time needed to accommodate the clock skew for the synchronization of the clock signal among the logic gates rises. While several approaches have been proposed to minimize the clock skew, delay lines are usually employed in the critical nets of packages, or printed circuit boards (PCBs). An example of this is the serpentine delay line routing scheme, as depicted in Fig. 1(a). Intuitively, it can be seen that the total time delay should be proportional to the total length of the delay line. However, crosstalk noise induced by the closely packed transmission line sections may cause significant deterioration in the total time delay and even result in the false switching of logic gates, especially for a serpentine delay line. Although a flat spiral delay line has better signal integrity than a serpentine delay line, it also exhibits some crosstalk noise on the time-domain transmission (TDT) waveform [1]–[3].

Guard traces, which are conductor lines grounded by a few plated via holes, are employed to diminish crosstalk between adjacent conductor paths in PCBs, or packages. However, it has been shown that this crosstalk reduction is constrained by certain design parameters [4]–[7].

A microstrip serpentine delay line, with the guard traces inserted into the cross-coupled conductors in the parallel section, has been proposed in order to improve the frequency characteristics of the delay line [8]. Further, in the TDT waveform and eye diagram of the guard traces embedded serpentine delay line routing scheme, as depicted in Fig. 1(b), it has been shown that the guard traces and the serpentine structure greatly reduce crosstalk for microstrip line structure [9], [10]. The ringing noise, due to the guard trace between two shorting vias in the microstrip line, can be suppressed by using only two grounded vias for the serpentine delay line structure [10]. However, this is difficult to accomplish using present manufacturing technology because the size of the pad of the grounded via surrounded by the bent trace of the serpentine routing scheme is larger. Although some layout changes are employed for the grounded via pad in the serpentine routing scheme, the overall scheme must meet the minimum layout requirements and requires strict control of the manufacturing process.

In previous studies [11], [12], it was found that the insertion of an open-stub type guard trace (OSGT) can result in a great deal of extra crosstalk noise in parallel coupled strip lines and just a few shorting vias of a guard trace can result in a large ringing noise in parallel coupled microstrip lines. This paper still proposes crosstalk noise reduction for the TDT waveform and eye diagram of an embedded microstrip serpentine delay line by using OSGTs. The OSGTs denotes the guard traces of one end is a grounded via while the other is open-ended and

Manuscript received February 12, 2011; revised July 24, 2011; accepted September 9, 2011. Date of publication October 14, 2011; date of current version November 8, 2011. This work was supported in part by the National Science Council of Taiwan under Grant NSC 98/99-2221-E-033-014, Grant CYCU-EECS, and Grant CYCU-EECS-9903, and MPI Corporation under Grant 99-09-03. Recommended for publication by Associate Editor S. L. Dvorak upon evaluation of reviewers' comments.

The authors are with the Department of Electronics Engineering, Chung Yuan Christian University, Taoyuan 32023, Taiwan (e-mail: ghs.apemc@msa.hinet.net; gahong94@cycu.org.tw; ghs@cycu.edu.tw; cmhsu@cycu.org.tw).

Color versions of one or more of the figures in this paper are available online at http://ieeexplore.ieee.org.

Digital Object Identifier 10.1109/TCPMT.2011.2168223

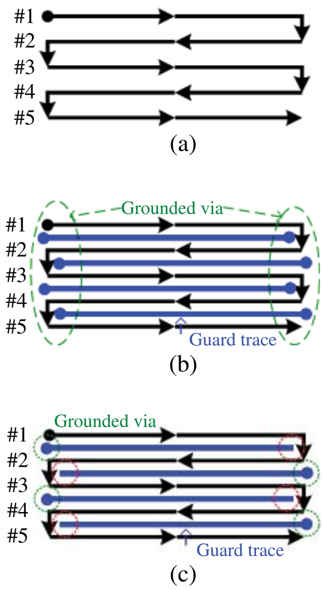

Fig. 1. Typical routing scheme for a serpentine delay line routing scheme for $N = 5$. (a) Without guard traces. (b) With two-grounded-via type guard traces (TGVGTs). (c) With OSGTs.

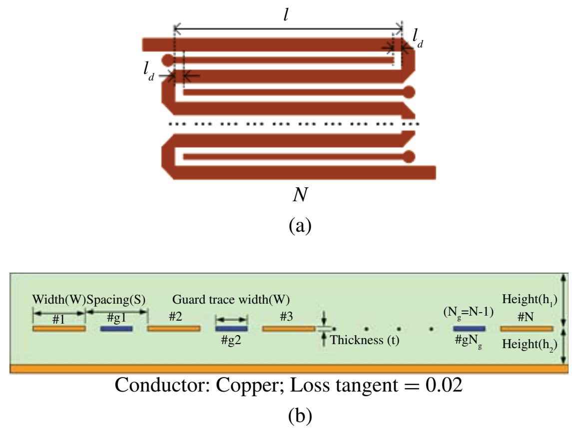

Fig. 2. (a) Top view and (b) cross-sectional view of the serpentine delay lines, with OSGTs inserted, detailing various parameters in the embedded microstrip structure.

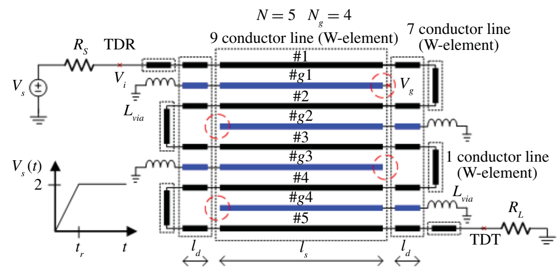

Fig. 3. Graphical configuration of the simulation method used in HSPICE for a serpentine delay line with OSGTs. (For $N = 5$).

located at a position where it is surrounded by the bent trace of a serpentine delay line, as shown in Fig. 1(c). Because the open ends substitute the grounded vias, which are surrounded by the bent trace, the scheme is easy to implement. The reduction in efficiency due to crosstalk noise, using OSGTs, occurs when using TGVGTs in the time-domain.

By extending the idea [13], this paper provides a more comprehensive investigation of serpentine routing scheme in an embedded microstrip structure. The organization of this paper is as follows. In Section II, the circuit model for serpentine delay line with guard traces is constructed. The comparison of TDT waveforms for serpentine delay line using TGVGTs and OSGTs is presented. Subsequently, the noise cancellation mechanism for OSGTs and the ringing crosstalk noise on the TDT waveform are fully explained using a graphic method. Section III focuses on the investigations of parameters which affect the noise cancellation and ringing crosstalk noise on the TDT waveform. The graphs for estimating the maximum flat voltage level of laddering wave [1] and the simple design guidelines for serpentine delay line using OSGTs are presented. Comparisons between simulated and measured results and between measured eye diagrams for different conditions are presented for verification in Section IV, followed by brief conclusions in Section V.

II. Modeling and Analysis of the Noise Cancellation Mechanism for Serpentine Delay Line with OSGTs

A. Model Setup

A typical serpentine delay line formed by embedded coupled microstrip lines with OSGTs is shown in Fig. 1(c). Fig. 2 shows the top and cross-sectional view of the serpentine delay line, depicting all structural parameters, a line with (W), length (λ) of parallel traces, section number of serpentine trace (N) $(N \geq 3)$, section number of guard trace (N_g) $(N_g = N - 1)$, guard trace width (W_g), spacing between coupled lines (S), trace thickness (t), substrate height (h_1, h_2), loss tangent $=$ 0.02, and dielectric constant (ε_r).

Fig. 3 shows the circuit model used in the HSPICE simulation for a serpentine delay line with guard traces inserted. The multiple coupled transmission lines, as well as the guard traces, are modeled by W-elements, thereby taking into account the finite transmission line loss. In addition, the vertical traces of the delay line are also modeled by W-elements. The small delay time at bends is considered, because it still slightly influences the noise cancellation mechanism. This is explained in the following section. The discontinuity effect of a bend can be neglected, because mitered bends are used [14]. The geometric length of a bend can be regarded as the time delay and be included in the length of the vertical traces to the approach. The grounded via of OSGTs is regarded as a series inductance [15]

$$L_{via} = \mu_0 \frac{h_{via}}{2\pi} \left[\ln\left(\frac{2h_{via}}{r_{via}} + \sqrt{1 + \left(\frac{2h_{via}}{r_{via}}\right)^2} \right) - \sqrt{1 + \left(\frac{r_{via}}{2h_{via}}\right)^2} + \frac{r_{via}}{2h_{via}} + \frac{1}{4} \right] \quad (1)$$

where h_{via} and r_{via} are denoted the height and radius of the grounded via, respectively.

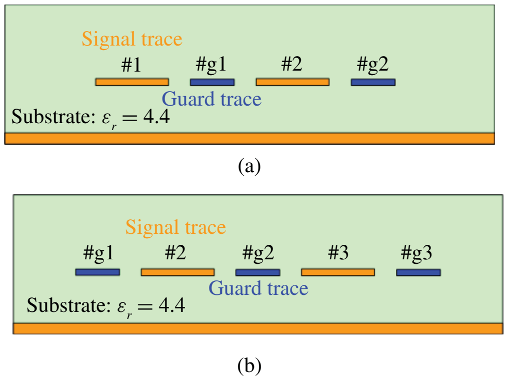

Fig. 4. Cross-sectional view of the two types of parallel lines with inserted guard traces for a serpentine delay line in an embedded microstrip structure (a) pattern 1 and (b) pattern 2.

B. Serpentine Delay Line with/without TGVGTs

Consider the serpentine delay line formed by coupled microstrip lines in Fig. 1(a). It is known that the near-end crosstalk (NEXT) V_n among the sections of a serpentine delay line accumulates in phase to appear as a laddering wave on the TDT waveform [1]. The maximum voltage level of the laddering wave approximates to $V_{\text{laddering,max}} = (N-1) \times V_n$. It is well known that the saturated NEXT levels in the victim line in the weak coupling state can be formulated as [15], with respect to the input voltage, V_i

$$V_n = V_i \times \frac{1}{4}\left(\frac{L_m}{L_S} + \frac{C_m}{C_S}\right) = V_i \times k_{\text{near}} \qquad (2)$$

in which k_{near} is the backward coupling coefficient, L_m is the mutual inductance, L_S is the self-inductance, C_m is the mutual capacitance, and C_S is the self-capacitance. The accumulation of crosstalk will deteriorate the TDT waveform, eye opening and jitter [3].

Because a guard trace is traditionally employed in reducing crosstalk noise between adjacent traces, a serpentine delay line with guard traces inserted between the parallel lines [Fig. 1(b)] is examined [9]. The maximum voltage level of the laddering wave approximates to

$$V_{\text{laddering,max}} = V_i \left(2 \times k_{\text{near},g\_1} + (N-3) \times k_{\text{near},g\_2}\right) \qquad (3)$$

where k_{near,g_1} and k_{near,g_2} denote the backward coupling coefficients for parallel lines with additional guard traces for patterns 1 and 2, respectively, as shown in the cross-sectional view in Fig. 4. Patterns 1 and 2 are the two sets of multiple parallel lines, with inserted guard traces, which yield a reduction in crosstalk noise for a serpentine delay line. The structure reduces crosstalk and results in an improved TDT waveform and eye diagram [9], [10].

C. Serpentine Delay Line with OSGTs

Here, it considers a serpentine delay line with OSGTs, as shown in Fig. 1(b), in the cross-sectional view, in Fig. 2, $W = 1.2$ mm, $S = 1.8$ mm, $h_1 = 3.2$ mm, $h_2 = 0.8$ mm, $t = 0.035$ mm, $W_g = 0.6$ mm, section number $N = 5$ ($N_g = 4$), $r_{via} = 0.7$ mm ($L_{via} = 0.186$ nH), $\ell_d = 1.2$ mm, loss

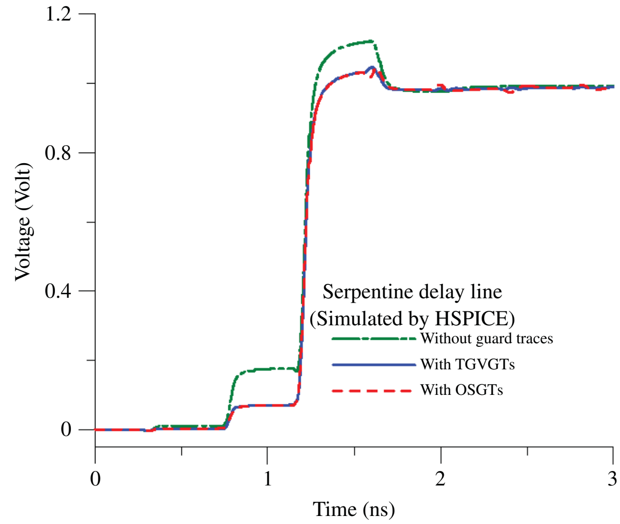

Fig. 5. Comparison of the simulated TDT waveforms for serpentine delay line without and with different type guard traces using HSPICE.

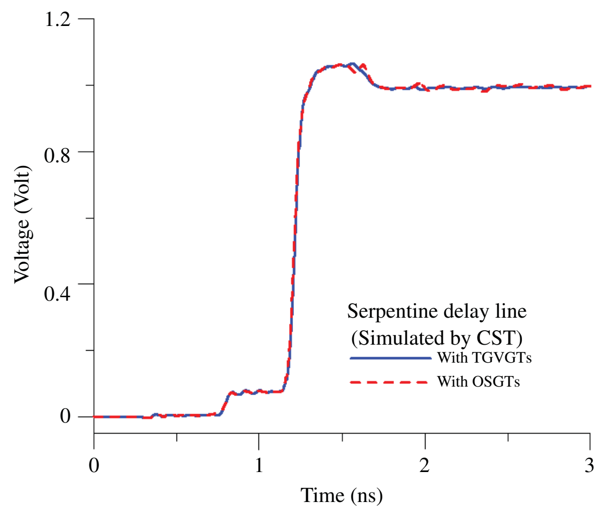

Fig. 6. Comparison of the simulated TDT waveforms for a serpentine delay line with TGVGTs and one with OSGTs using the computer simulation technology (CST) simulator.

tangent $= 0.02$, $\varepsilon_r = 4.4$, and $\ell_s = 28.8$ mm. The effective dielectric constant of this embedded microstrip structure is about 4.35. Moreover, the inductive coupling factor (L_m/L_s) approaches capacitive coupling factor (C_m/C_s) because the effective dielectric constant approaches the dielectric constant (4.4) of the substrate. Therefore, the far-end crosstalk noise is only slight and is thus neglected in this paper.

The driver and load resistances are chosen as $R_S = R_L = 50\ \Omega$ and the rise time of the source $V_S(t)$ is 50 ps. Using the HSPICE circuit model the TDT waveforms for a serpentine delay line with TGVGTs/OSGTs, but without guard traces, is simulated, as shown in Fig. 5. Though there is slight deviation in the high flat voltage level of the TDT waveform, it is obvious that the simulated results of the TDT waveforms for a serpentine delay line with OSGTs and one with TGVGTs are almost the same. Compared with the serpentine delay line without guard traces, the serpentine delay line with OSGTs or

TABLE I
MAXIMUM FLAT VOLTAGE LEVELS OF THE LADDERING WAVE FOR A SERPENTINE DELAY LINE USING BOTH ADDITIONAL TGVGTs AND OSGTs OBTAINED USING FORMULA, HSPICE AND CST SIMULATION

	$V_{\text{laddering,max}}$	
Approximation Formula	72.69 mV	
	Additional TGVGTs	Additional OSGTs
HSPICE Simulation (loss tangent = 0.02, Copper)	70.53 mV	70.19 mV
CST Simulation (loss tangent = 0.02, Copper)	70.35 mV	70.89 mV

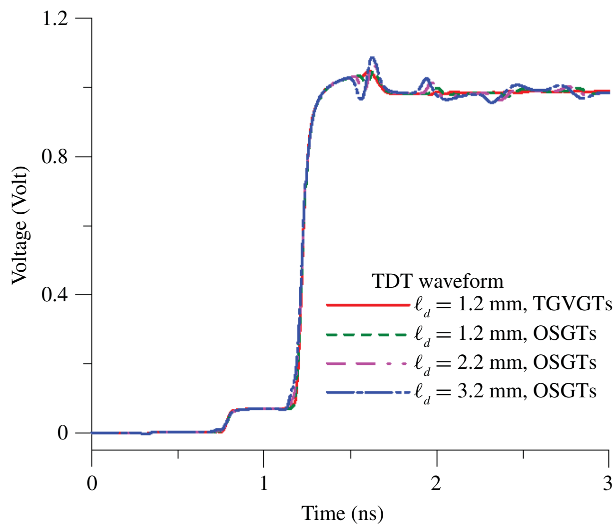

Fig. 7. Comparison of the simulated TDT waveforms of a serpentine delay line with OSGTs for different ℓ_d.

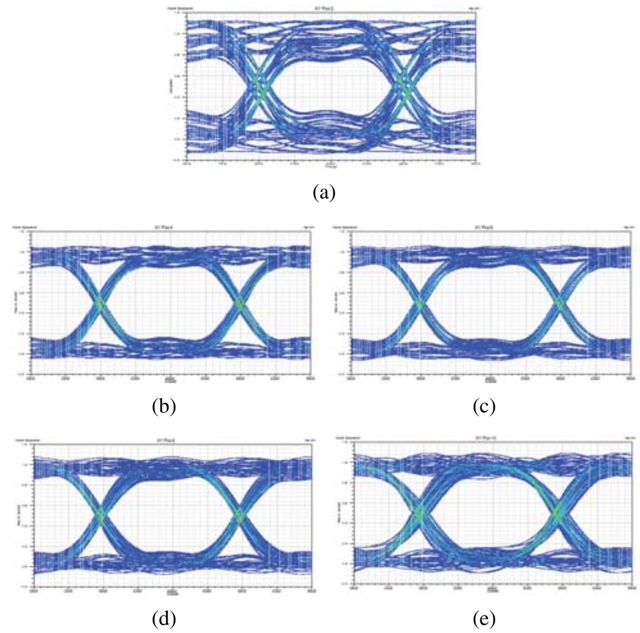

Fig. 8. Comparison of the simulated eye diagrams, for a serpentine delay line with/without TGVGTs/OSGTs, with a data ratio 5 Gb/s, for different ℓ_d conditions (a) without guard traces, (b) with $\ell_d = 1.2$ mm and TGVGTs, (c) with $\ell_d = 1.2$ mm and OSGTs, (d) with $\ell_d = 2.2$ mm and OSGTs, and (e) with $\ell_d = 3.2$ mm and OSGTs.

TABLE II
COMPARISON OF THE SIMULATED VALUES OF THE PARAMETERS OF THE EYE DIAGRAM FOR A SERPENTINE DELAY LINE WITH/WITHOUT TGVGTs AND OSGTs WITH DIFFERENT l_d

Data ratio = 5 Gb/s	w/o GTs	l_d = 1.2 mm, TGVGTs	l_d = 1.2 mm, OSGTs	l_d = 2.2 mm, OSGTs	l_d = 3.2 mm, OSGTs
Eye open (mV)	454.68	694.77	698.37	689.14	672.66
Eye width (ps)	170.77	187.43	187.13	185.49	176.75
jitter (ps)	32.79	16.53	16.53	18.72	27.6

TGVGTs exhibits a significant reduction in crosstalk noise. The maximum flat voltage level of the laddering wave is reduced from 0.1746 V to 0.0702 V, which represents a 60% reduction. Fig. 6 shows the simulated TDT waveforms for a serpentine delay line with OSGTs and TGVGTs, obtained using CST, 3-D full-wave simulator [16]. It can be seen that the results are similar to the HSPICE simulated results, except for the slight deviation on the high flat voltage level of the TDT waveform. Both simulations of the TDT waveforms for a serpentine delay line with OSGTs or TGVGTs show agreement. Comparing the simulation results for TDT waveforms, in Figs. 5 and 6, for a serpentine delay line with OSGTs also shows agreement. Table I lists the predicted values for HSPICE and CST simulations. There is good agreement between formula and simulations for the maximum flat voltage level of the laddering wave. Furthermore, the maximum voltage levels of the laddering wave for a serpentine delay line approach those for the addition of TGVGTs and OSGTs.

Fig. 7 shows the results of the simulated TDT waveforms for a serpentine delay line with OSGTs for different ℓ_d. A pseudorandom incident signal with a rise/fall time 50 ps, data rate of 5 Gbs, and voltage swing of 2 V is utilized to simulate the eye diagram. Fig. 8 shows the comparison of the simulated eye diagrams for a serpentine delay line with/without TGVGTs/OSGTs for different ℓ_d using HSPICE and Designer [16] simulation. According to Fig. 8, Table II lists the simulated values of the parameters of the eye diagrams. It is obvious that there is ringing crosstalk noise (V_r) on the TDT waveforms, due to large ℓ_d, as shown in Fig. 7. This large ℓ_d leads to the large ringing crosstalk noise and bad eye diagram, as shown in Fig. 8. In Table II, with an increasing ℓ_d, the eye opening and eye width are reduced. The jitters become significantly larger. According to Fig. 7, the large the maximum flat voltage levels for the laddering wave are almost the same value for different ℓ_d.

D. Crosstalk Noise Cancellation Mechanism on OSGTs

It considers the same structural parameters as in Fig. 2, the simulated crosstalk noises for embedded coupled microstrip lines with OSGT are shown in Fig. 9. Because one end of guard trace is open, there is increased crosstalk noise on the OSGT. This also induces increased crosstalk noises not only at the near-end but also at the far-end [11], as shown in Fig. 9. However, the increased crosstalk noises are almost

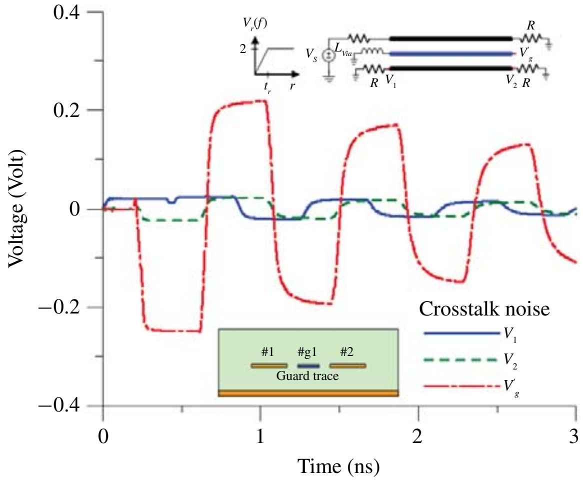

Fig. 9. Simulated crosstalk noises for embedded coupled microstrip lines with OSGTs.

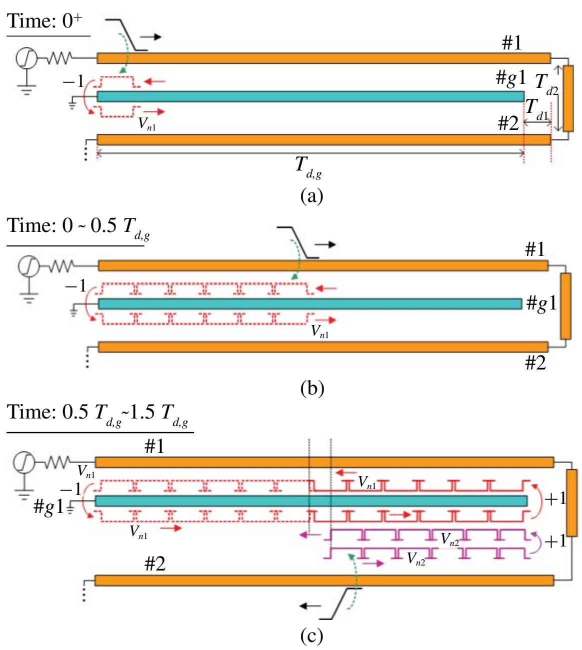

Fig. 10. Using the graphic method, the summary of the propagation of crosstalk noises on the OSGT #$g1$ at time (a) 0+, (b) $0 \sim 0.5T_{d,g}$, and (c) $0.5T_{d,g} \sim 1.5T_{d,g}$.

absent from the TDT waveform for a serpentine delay line with OSGTs, especially for small ℓ_d. Notably, according to Fig. 9, the far-end crosstalk noises are very small and ignored in this embedded microstrip line structure.

It is seen that, with the special serpentine routing scheme, OSGTs provide a crosstalk noise cancelation mechanism. A popular graphic method, to illustrate and predict the crosstalk waveforms for coupled transmission lines with matched termination, based on wave tracing was used [17]. Using this same graphic method, the crosstalk noise cancelation mechanism in OSGTs for embedded microstrip serpentine delay line can be illustrated. The following illustration considers the condition that the rise time is smaller than twice the delay time ($T_{d,g}$) of the OSGT. For simplicity, a lossless condition is assumed for

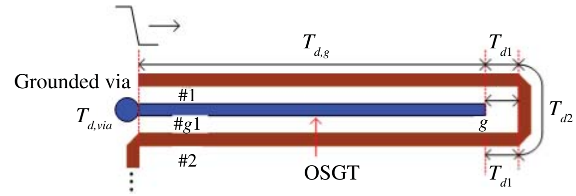

Fig. 11. Important parameters and partial structure for a serpentine delay line with OSGTs.

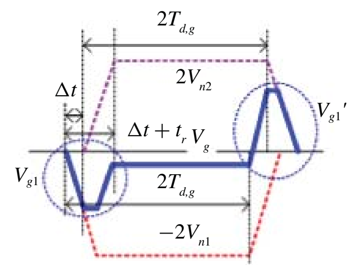

Fig. 12. Diagram of crosstalk noise cancelation mechanism for OSGT.

the structure and the grounded vias of the OSGT are regarded as ideal shorts only for the graphic method. V_{n1} and V_{n2} denote the backward crosstalk noise coupling on the OSGT from trace sections #1 and #2 of the serpentine delay line, respectively.

Consider a ramped step pulse (main signal) with amplitude $2V_i$ and rise time (t_r) propagating down the trace section #1 of the serpentine delay line, as shown in Fig. 10(a). The backward propagating crosstalk noise, V_{n1}, is immediately induced on the OSGT, #$g1$, through mutual capacitance and inductance, as shown in Fig. 10(a). At the same time, once V_{n1} reaches the shorting grounded via, at the left end, its polarity is reversed and it propagates toward the right end. Thus the crosstalk noise V_{n1}, toward both right end and left end, cancels each other during the time $0 \sim 1\ T_{d,g}$.

The V_{n1}, of reversed polarity, propagating toward the right end of the OSGT #$g1$, will encounter an open-end. Because the reflection coefficient of an open-end is 1, V_{n1} maintains its polarity (negative polarity) and propagates toward the left end of the OSGT #$g1$ during the time $1T_{d,g} \sim 2T_{d,g}$. Because the reflection coefficient is 1, the amplitude crosstalk noise becomes $2V_{n1}$ after time $1T_{d,g}$ at OSGT #$g1$.

After time $T_{d,g} + 2T_{d1} + T_{d2}$, the main signal propagates from right end to left end on trace section #2. The time delay T_{d2} includes both vertical line (T_{dv}) and bends ($2T_{d,\text{bend}}$). The main signal immediately induces another backward propagating crosstalk noise, V_{n2}, propagated to the right end of OSGT #$g1$ after time $T_{d,g} + 2T_{d1} + T_{d2}$. When this V_{n2} encounters the open-end, V_{n2} immediately becomes $2V_{n2}$ and propagates from the right end of OSGT #$g1$ to the left end. Because the voltage polarity is reversed, the two backward crosstalk noises, $2V_{n1}$ and $2V_{n2}$, cancel each other in the majority, as shown in Fig. 10(c). Each pair of signal traces in a serpentine delay line with one OSGT follows this signal propagation procedure, so, the signal propagation procedure repeats until the main signal propagates through the serpentine delay line.

Based on the above simple graphic depiction, more practical conditions and parameters, such as $T_{d,via}$, g point and ℓ_d,

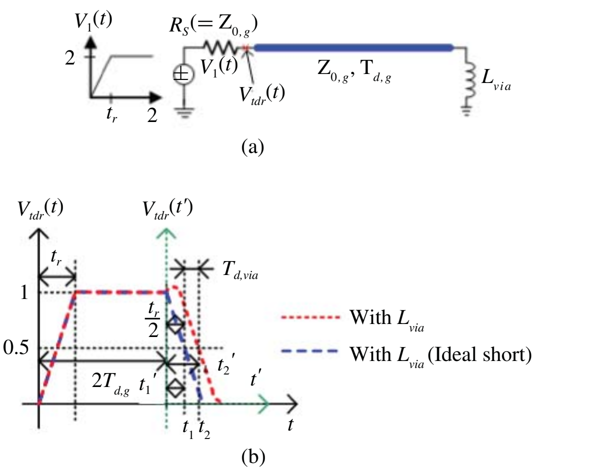

Fig. 13. (a) Circuit model for estimating the delay time for a grounded via. (b) Time-domain reflection (TDR) waveforms with and without L_{via}.

are considered and noted in Fig. 11. However, due to the serpentine bend routing scheme and grounded via, the two backward crosstalk noises do not cancel each other completely. For a rise time (t_r), for main signal, the simple diagram for crosstalk noise cancelation is shown in Fig. 12. The residual crosstalk noise is called V_g. The voltage V_g is detected at point g, the open-end of OSGT. The amplitude of V_g depends on the time difference Δt. Δt can be estimated by (4)

$$\Delta t = 2T_{d1} + T_{d2} - T_{d,via} = T_{\text{serp.\_bend}} - T_{d,via}. \quad (4)$$

The $T_{\text{serp.\_bend}}$ $(= 2T_{d1}+T_{d2})$ and $T_{d,via}$ are the delay times due to serpentine bend routing and grounded via, respectively. T_{d1} is the delay time of ℓ_d, which denotes the distance between the open-end of the OSGTs and the vertical trace of the serpentine bend routing section.

In order to verify the crosstalk noise cancelation mechanism for OSGTs, the estimated time difference Δt, T_{d1}, T_{d2}, and $T_{d,via}$, must be calculated. For the previous example, in Section II-C., the time delays T_{d1} and T_{d2} can be easily estimated to be about 8.3 ps and 19.1 ps, respectively. To evaluate the time delay ($T_{d,\text{via}}$) of a grounded via, a circuit model is detailed in Fig. 13(a). The grounded via is represented by an inductor L_{via}. A ramped step pulse with amplitude 2V and rise time (t_r) propagates down the trace, which is terminated with an inductor (L_{via}). The trace has the same characteristic impedance ($Z_{0,g}$) and time delay ($T_{d,g}$) as the OSGT. A comparison of the time-domain reflection (TDR) waveform, with and without L_{via}, is shown in Fig. 13(b). From the Fig. 13(b), the time delay ($T_{d,\text{via}}$) of the grounded via can be defined as the time difference between the arrival time of the reflected waveform at point r, with and without L_{via}. The waveform's arrival time is defined as the time of a half of the voltage amplitude 1 Volt. In general, the rise time (t_r) is larger than the time delay ($T_{d,\text{via}}$) of the grounded via. $V_{\text{tdr}}(r, t')$ at point r can be approximated by the formula [18]

$$V_{tdr}(r, t') = -\frac{1}{t_r}\left[2\tau\left(1 - e^{-\frac{t'}{\tau}}\right) - t' + t_r\right], \; 0 \le t' \le t_r \quad (5)$$

where $t' = t - 2T_{d,g}$ and is the time constant ($\tau = L_{via}/Z_{0,g}$). The time delay $T_{d,via}$ can be estimated with (6)

$$T_{d,via} = t_2' - t_1' = t'\big|_{V_{tdr}(r,t')=0.5} - \frac{1}{2}t_r. \quad (6)$$

From (5) and (6), the time delay for the inductance (0.186 nH) of the grounded via ($r_v = 0.7$ mm) is about 5.5 ps in the previous example.

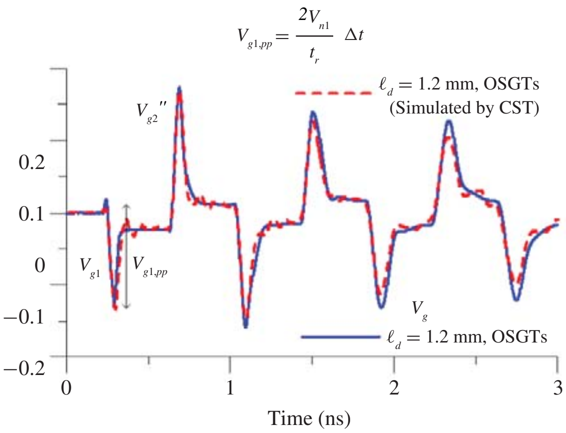

Fig. 14. Comparison of the V_g waveforms simulated by HSPICE and CST simulators.

TABLE III
COMPARISON OF RESULTS FOR THE AMPLITUDE OF THE FIRST PEAK VOLTAGE FOR RESIDUAL CROSSTALK NOISE V_{g1}, AT THE OPEN-END OF THE OSGT, USING AN APPROXIMATION FORMULA AND HSPICE SIMULATION

$l_d = 1.2$ mm	$V_{g1,pp}$
Approximation Formula	148.8 mV
HSPICE Simulation (loss tangent = 0, PEC)	146.5 mV
HSPICE Simulation (loss tangent = 0.02, Copper)	136.1 mV

Fig. 14 shows the comparison of the residual crosstalk noise V_g simulated by HSPICE and CST simulator [16]. It can be seen that the results are almost the same for each method. Table III lists the predicted peak-to-peak amplitude ($V_{g1,pp}$) of the first peak voltage and that found by HSPICE simulation. The good agreement between results shows that the amplitude of the first peak voltage on waveform V_g can be estimated by the approximation (5), which is derived from the diagram, Fig. 12, for a crosstalk noise cancelation mechanism, which is assumed to be lossless. The formula derived here, for lossless lines, also provides an upper bound for the peak-to-peak amplitude of the first peak voltage for waveform V_g, in lines with losses

$$V_{g1,pp} = \frac{2V_{n1}}{t_r}\Delta t. \quad (7)$$

E. Ringing Crosstalk Noise Generation on TDT Waveform

Because the ringing crosstalk noise on a TDT waveform, for a serpentine delay line with additional OSGTs (Fig. 7) is induced by the residual crosstalk noise V_g [11], the generation mechanism for the ringing crosstalk noise can also

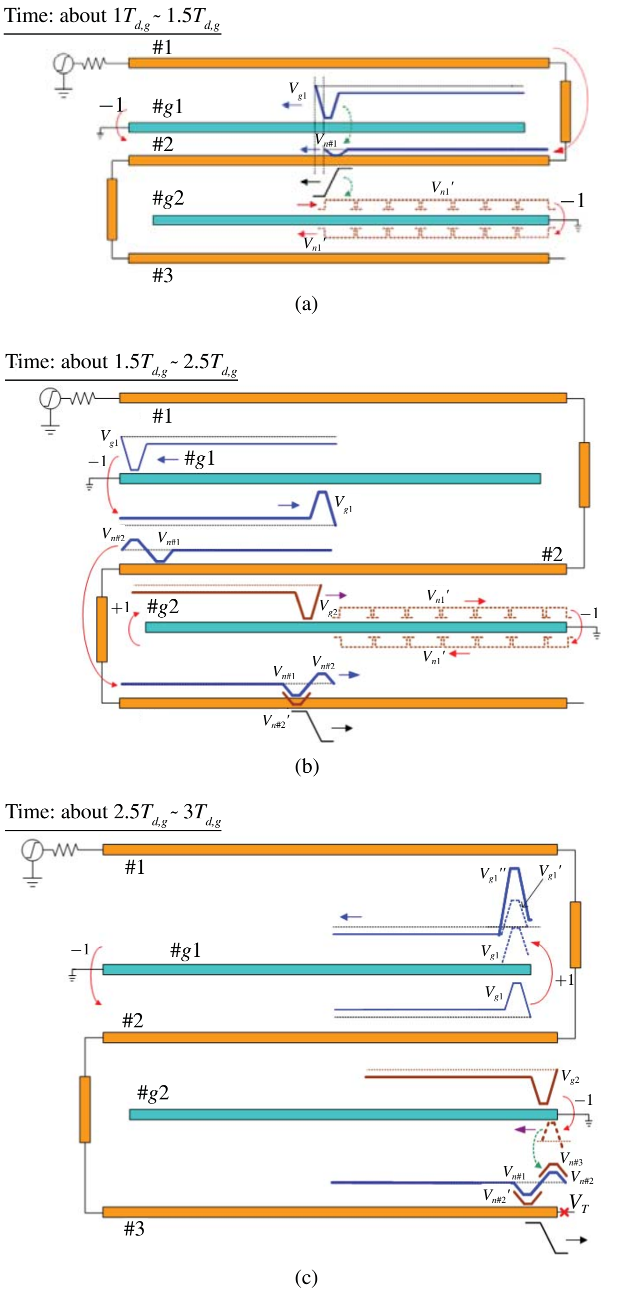

Fig. 15. Graphic summary of the generation mechanism for ringing crosstalk noise on the TDT waveform at time (a) about $1T_{d,g} \sim 1.5T_{d,g}$, (b) about $1.5T_{d,g} \sim 2.5T_{d,g}$, and (c) about $2.5T_{d,g} \sim 3T^{+}_{d,g}$.

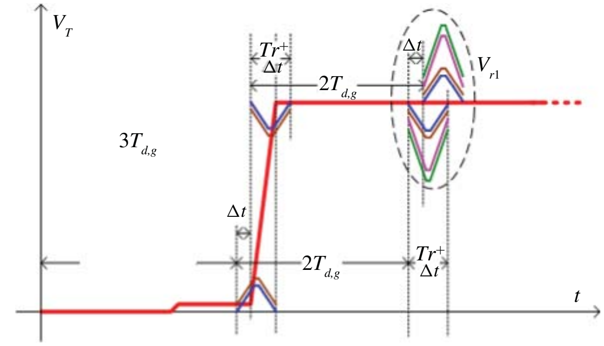

Fig. 16. Diagram showing the summary of ringing crosstalk noises on the TDT waveform.

be illustrated using the simple graphic method. From the above graphic illustration of the crosstalk noise cancelation mechanism for V_g, the resultant NEXT noise voltage V_g is used in the following graphic explanations. In addition, for simplicity, this graphic illustration only focuses on crosstalk noises induced in the TDT waveform.

The first voltage peak (negative polarity) V_{g1} propagates toward the left end of the OSGT $\#g1$ during the time $1T_{d,g} \sim 2T_{d,g}$. At the same time, a small NEXT noise $\upsilon_{n,\#1}$ on signal trace #1 is induced by V_{g1}. This noise $\upsilon_{n,\#1}$ propagates through the vertical signal trace and toward the left end of signal trace #2. During the time $(1T_{d,g}+2T_{d1}+1T_{d2}) \sim 2T_{d,g}$, the main signal propagates from the right end of trace #2 toward the left end and the other V'_{n1} is induced at OSGT $\#g2$. Once V_{g1} reaches the shorting grounded via, at the left end, its voltage polarity is reversed and it propagates toward the right end. At the same time, the small NEXT noise $\upsilon_{n,\#2}$ is immediately induced in signal trace #2. Due to the delay time $T_{\text{serp.\_bend}}$ for $\upsilon_{n,\#1}$, the timing sequence for the two induced noises is $\upsilon_{n,\#2}$, $\upsilon_{n,\#1}$. The graphic illustration is shown in Fig. 15(b). At time $2T_{d,g} + T_{\text{serp.\_bend}} - T_{d1}$, the first voltage peak (negative polarity) V_{g2} of the other resultant NEXT noise voltage appears at the open end of OSGT $\#g2$. At the same time, the small NEXT noise $\upsilon'_{n,\#2}$ is immediately induced in signal trace #2. The noise $\upsilon'_{n,\#2}$ appears at almost the same time as noise $\upsilon_{n,\#1}$. The three induced noises $\upsilon_{n,\#2}$,$\upsilon_{n,\#1}$ and $\upsilon'_{n,\#2}$ propagate through the vertical signal trace and toward the right end of signal trace #3, as shown in Fig. 15(b). After time $3T_{d,g}+T_{d1}+T_{d2}$, the voltage V_{g2} propagates toward the right end of OSGT $\#g2$. Once V_{g2} reaches the shorting grounded via, at the right end, its voltage polarity is reversed and it propagates toward the left end. At the same time, the small NEXT noise $\upsilon_{n,\#3}$ is immediately induced in signal trace #3. Because of the delay time $T_{\text{serp.\_bend}}$ for $\upsilon_{n,\#2}$,$\upsilon_{n,\#1}$ and $\upsilon'_{n,\#2}$, the noise $\upsilon_{n,\#3}$ appears almost at the same time as noise $\upsilon_{n,\#2}$. A graphic illustration is shown in Fig. 15(c).

At about the time $3T^{+}_{d,g}$, the voltage peak (positive polarity) V_{g1} is superimposed upon the voltage peak (positive polarity) V'_{g1}. The resultant voltage of the two voltage peaks is V''_{g1}, as shown in Fig. 15(c). After about time $3T_{d,g}$, the voltage peak V''_{g1} propagates back and forth in the OSGT. In the simple graphic illustration of the generation mechanism, ringing crosstalk noise is only induced by the first voltage peak (negative polarity) V_{g1} for a serpentine delay line ($N = 3$) with OSGTs. The generation mechanism for the following ringing crosstalk noise, induced by other voltage peaks on the OSGTs, adheres to the above signal sequence.

Fig. 16 shows the diagram of a TDT waveform. The four small crosstalk noises, $\upsilon_{n,\#3}$, $\upsilon_{n,\#2}$, $\upsilon'_{n,\#2}$, and $\upsilon_{n,\#1}$(also called first group of induced ringing crosstalk noises), induced by the first peak voltages, V_{g1} and V_{g2}, appears at about the time $3T_{d,g}+1T_{d1}+1T_{d2}$. It is obvious that the positive and negative polarity crosstalk noises, in the first group of induced ringing crosstalk noise, cannot completely cancel each other due to the time difference Δt shown in Fig. 16.

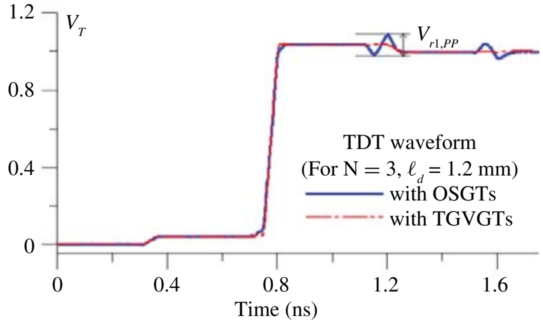

Fig. 17. Comparisons of the TDT waveforms for a serpentine delay line ($N = 3$, $N_g = 2$) with OSGTs and TGVGTs simulated by HSPICE under lossless and $L_{via} = 0$ assumptions.

It is well known that a narrow positive incident voltage pulse, transmitted in parallel coupled lines, results in narrow NEXT noises - the sum of two voltages of opposite polarity and a time difference of about double the delay time of the parallel coupled lines between them. Therefore, the other four small crosstalk noises (also called the second group of induced ringing crosstalk noises) are also induced by the first peak voltages, V_{g1} and V_{g2}, but the voltage polarity is revised, as compared with the first group of induced ringing crosstalk noises shown in Fig. 15. With reference to the graphic illustration of the generation mechanism of ringing crosstalk noises on a TDT waveform, it can be seen that the other four large ringing crosstalk noises (also called the third group of induced ringing crosstalk noises), induced by V''_{g1} and V''_{g2}, appear at about the time $5T_{d,g} + 1T_{d1} + 1T_{d2}$. Because of the serpentine routing scheme with OSGTs, voltage peaks of the same voltage polarity as the second and third groups of induced ringing crosstalk noises have almost the same time to superimpose. However, from Fig. 16, it is obvious that the resultant crosstalk noise (also called ringing noise, V_{r1}) of the positive and negative polarity crosstalk noises in the second and third groups of induced ringing crosstalk noises also cannot completely cancel each other due to the time difference Δt. This explains the small ℓ_d and the small amplitude of ringing crosstalk noise in Fig. 7.

Fig. 17 shows a comparison of the TDT waveforms for a serpentine delay line ($N = 3$, $N_g = 2$) with OSGTs and TGVGTs, simulated by HSPICE under lossless and $L_{via} = 0$ assumptions. Table IV lists the predicted peak-to-peak amplitude ($V_{r,pp}$) of the V_{r1} and that found by HSPICE simulation. The good agreement shows that peak-to-peak amplitude of the V_r on a TDT waveform can be estimated by the approximation (2), (5) and simple algebraic calculation. Hence, the generation mechanism of ringing crosstalk noises in a TDT waveform can be verified. However, due to losses and signal energy scatter, the difference in amplitude of $V_{r,pp}$ between the loss and lossless conditions is large in this case. This is an advantage for a designer wishing to use this structure. For more section numbers, the peak-to-peak amplitude ($V_{r,pp}$) of the V_{r1}becomes large in accordance with the procedure for the generation of ringing crosstalk noises in the TDT waveform.

TABLE IV
COMPARISON OF THE PEAK-TO-PEAK AMPLITUDE OF V_r IN TDT WAVEFORMS OBTAINED USING THE APPROXIMATION FORMULA AND HSPICE SIMULATION

For $N = 3$, $N_g = 2$, $l_d = 1.2$ mm	$V_{r1,pp}$
Approximation Formula	73.5 mV
HSPICE Simulation (loss tangent = 0, PEC)	73.0 mV
HSPICE Simulation (loss tangent = 0.02, Copper)	33.1 mV

TABLE V
COMPARISON OF THE MEASURED VALUES OF EYE DIAGRAM PARAMETERS FOR A SERPENTINE DELAY LINE WITH/WITHOUT TGVGTs AND OSGTs

Measured eye diagram	Data ratio = 5 Gb/s			Data ratio = 7.5 Gb/s		
	w/o GTs	With TGVGTs	With OSGTs	w/o GTs	With TGVGTs	With OSGTs
Eye open (mV)	179	267	269	154	256	251
Eye width (ps)	158	174	172	84	103	103
jitter (ps)	43	27	27	50	30	31

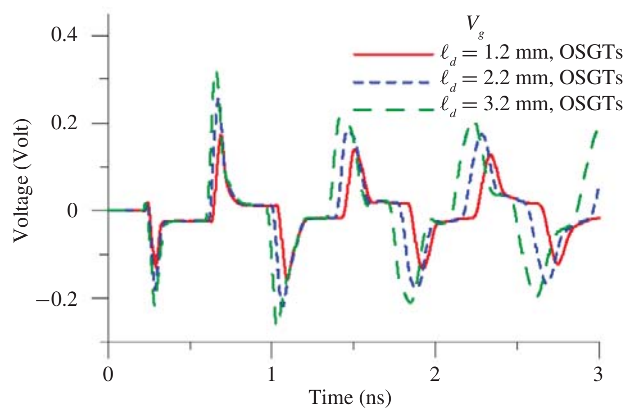

Fig. 18. Comparison of simulated voltage waveform V_g at point g on the OSGT for different ℓ_d.

III. SIMULATED RESULTS OF NOISE CANCELLATION AND TDT WAVEFORM FOR A SERPENTINE DELAY LINE WITH OSGTs

As has already been demonstrated, in order to obtain the minimum ringing crosstalk noise in a TDT waveform, the time difference Δt in (4) must be minimum. A minimum Δt means decreasing the delay time $T_{serp.\_bend}$ and increasing the delay time $T_{d,via}$. These two delay times are considered in the following section.

Decreasing the delay time $T_{serp.\_bend}$ also means decreasing T_{d1} and T_{d2}. In other words, ℓ_d and S must be minimized. The following example analysis is based on the example in Section II-C. Fig. 18 shows the simulated waveforms for voltage V_g, with different ℓ_d, on the open end of OSGT #$g1$. It is obvious that the smaller ℓ_d becomes the larger is the amount of noise cancelation and the smaller is the voltage amplitude V_g. For the generation of ringing crosstalk as seen in Section II, the smaller the voltage amplitude V_g, the

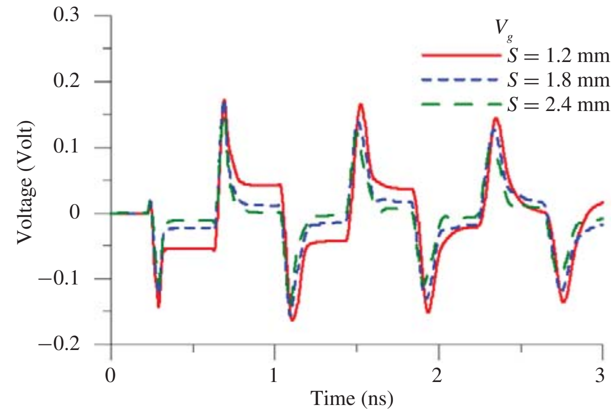

Fig. 19. Comparison of simulated voltage waveform V_g at point g on the OSGT for different S.

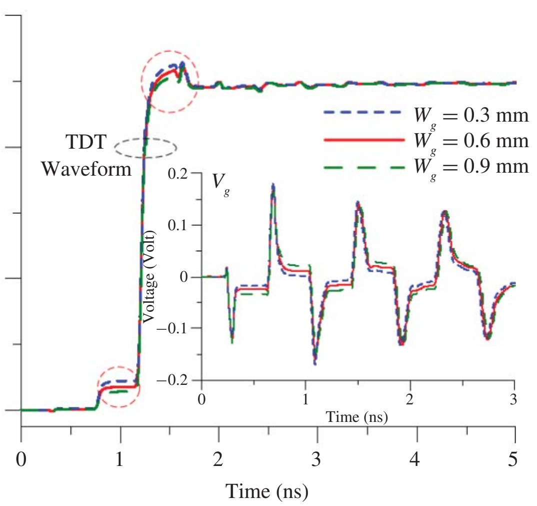

Fig. 20. Comparison of simulated V_g and TDT waveform of a serpentine delay line with OSGTs for different W_g.

smaller is ringing crosstalk noise, as shown in Figs. 7 and 18. When the amount of noise cancellation is large, the two TDT waveforms for OSGTs and TGVGTs look most alike.

Fig. 19 shows the simulated waveforms for voltage V_g with different S. From aforementioned studies of noise cancelation mechanisms, it is known that larger S results in larger T_{d2} and Δt, so the amplitude of V_g becomes large. Nevertheless, because the effect of crosstalk noise coupling on the OSGT dominates the crosstalk noise cancelation mechanism, it is obvious that as S becomes larger, V_g becomes smaller, as shown in Fig. 19. Consequently, for small S, the crosstalk noise voltage V_g cannot be minimized. Because the amplitude difference for V_g is not large, the TDT waveforms are not shown in here.

Fig. 20 presents the simulated V_g and TDT waveforms for different widths of OSGTs. It can be seen that the trace width of OSGTs affects the coupling strength between sections of the serpentine delay line. Therefore, from Fig. 20, the sections of accumulated NEXT noises on the TDT waveforms, which are circled with a red dotted line, become large for small trace widths of OSGTs. In addition, because the chosen range

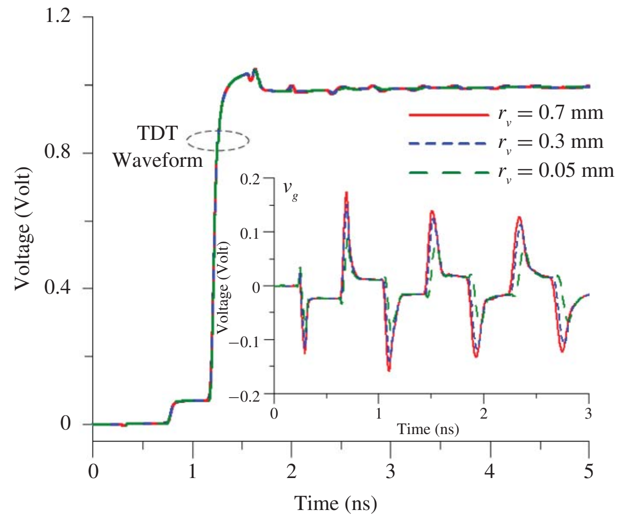

Fig. 21. Comparison of simulated V_g and TDT waveform of a serpentine delay line with OSGTs for different r_v.

of trace widths of the OSGTs has almost no effect on the voltage V_g for the same ℓ_d, the ringing crosstalk noises on TDT waveforms look alike.

Fig. 21 shows a comparison of simulated V_g and TDT waveforms of serpentine delay line with OSGTs for different radius (r_v) of grounded via. Because only the radius of the grounded via is changed, the maximum flat voltage level of the laddering wave on the TDT waveforms almost maintains the same value. Obviously, the smaller the radius of grounded via, the smaller is the amplitude of voltage V_g. Because the small radius results in a large inductance (L_{via}) for the grounded via and large delay time ($T_{d,via}$), the time difference (Δt) becomes small and the voltage V_g also becomes small, as dictated by (4). Although the amplitude of voltage V_g is significantly reduced, for $r_v = 0.05$ mm, there is little reduction in ringing crosstalk noise in the TDT waveform. Nevertheless, even if using a small radius for the grounded via produces only a small reduction in crosstalk noise, the TDT waveform still maintains good signal quality and integrity.

It is worth mentioning that this paper shows that the resultant crosstalk noise voltage V_g has almost no effect on the maximum flat voltage level of the laddering wave on a TDT waveform, as shown in Figs. 7 and 21. The crosstalk noise voltage V_g only almost affects the magnitude of the ringing crosstalk noise on the TDT waveform. Therefore, the value for the maximum flat voltage level of a laddering wave, for a serpentine delay line with OSGTs, approaches that for a serpentine delay line with TGVGTs.

Although (2) and (3) provide a means of quantitative analysis, for the evaluation of the magnitude of TDT crosstalk noise reduction, it would be time-consuming to repeat the process, if the layout of serpentine delay line with OSGTs is redesigned. The graphs of TDT crosstalk noise versus the dimension for serpentine delay line with OSGTs might prove more useful in this case. As shown, in Fig. 22, with reference to (3), in general, the total coupling degree of TDT crosstalk noise is the sum of the two parts of patterns 1 and 2. The coupling degrees of TDT crosstalk noise are normalized by

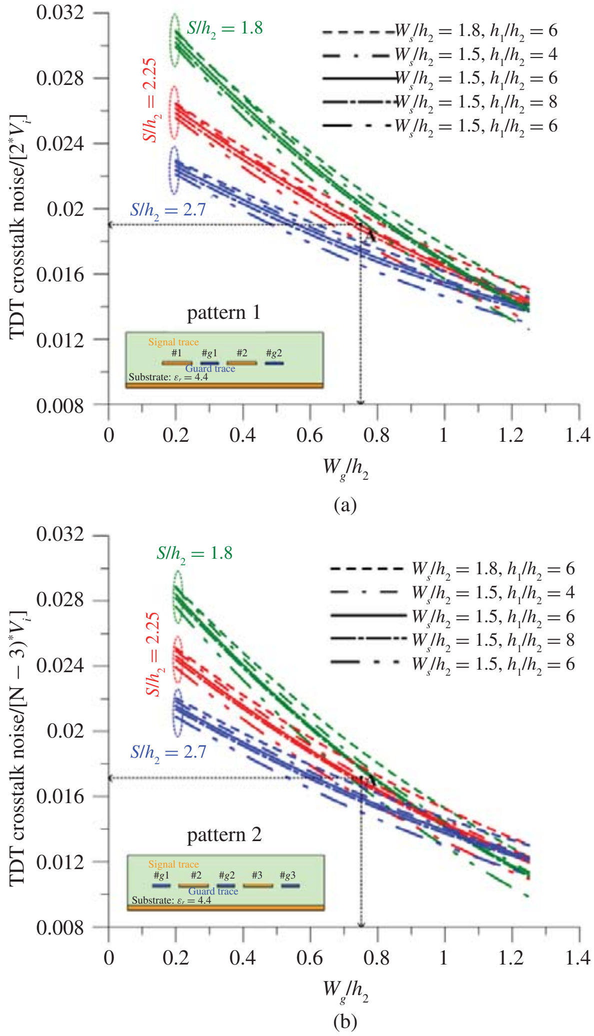

Fig. 22. Graph of TDT crosstalk noise versus the physical dimension of the serpentine delay line with OSGTs (a) for pattern 1 and (b) for pattern 2.

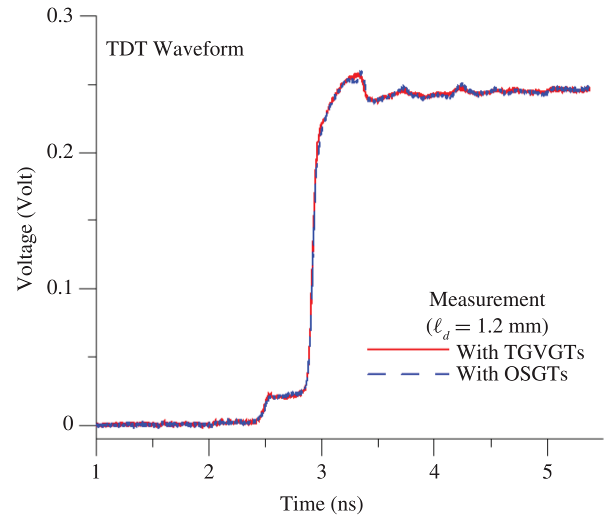

Fig. 23. Comparison of measured TDT waveforms for serpentine delay lines using TGVGTs and OSGTs.

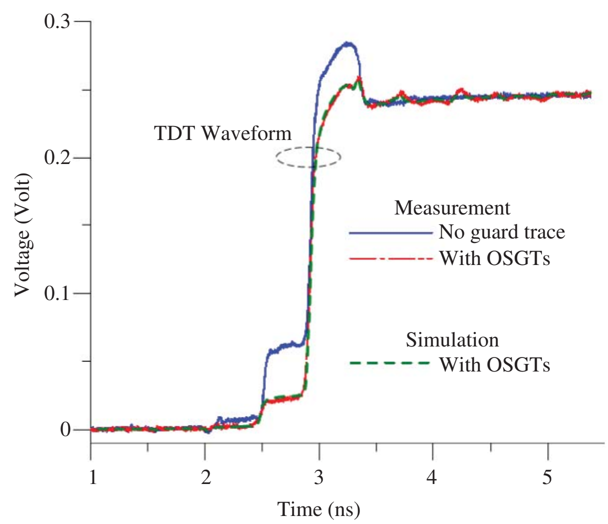

Fig. 24. Comparison of measured TDT waveforms and the simulated results for a serpentine delay line with/without OSGTs.

$2 * V_i$ and $(N-3) * V_i$, for patterns 1 and 2, respectively. In Fig. 22, the point A represents the example in Section II-C. Using this graph, it is easy to estimate the maximum flat voltage level of a laddering wave for a serpentine delay line with OSGTs.

Our study provides the following simple guidelines for the use of OSGTs in the reduction of crosstalk noise and maintenance of a good TDT waveform and eye diagram for a serpentine delay line in an embedded microstrip structure, (1). To estimate the maximum flat voltage level of laddering wave on TDT waveform, OSGTs can be assumed to be ideal ground lines. The value of this maximum flat voltage is almost equivalent to that for the use of TGVGTs (2). Using the smallest ℓ_d and radius (r_v) of grounded via can help to ensure a minimum of ringing crosstalk noise on the TDT waveform.

In addition, it is worthy of note that far-end crosstalk can be ignored in a stripline structure because it is homogeneous environment. So, the OSGTs can also be inserted in a serpentine delay line in the stripline structure to improve the TDT waveform and eye diagram.

IV. Experimental Validation

To verify that the proposed structure yields a useful improvement in TDT waveforms and eye diagrams, the TDT waveforms were measured and compared to the simulated results. The eye diagrams were also measured for the purposes of comparison. The embedded microstrip serpentine delay line, in Fig. 2(a), has seven sections ($N = 7$, $N_g = 6$), $\ell_d = 1.2$ mm and a cross section as shown in Fig. 2(b). In addition, for ease of manufacture of the test board, in our laboratory, the radius of the grounded via was 0.3 mm. The other physical parameters were almost the same as the example in Section II-C. The experiment was performed on a time-domain reflectometer, TEK/CSA8000, with both source and load resistances of 50 Ω. The reflectometer provided the source of the launching voltage for HSPICE simulation.

Fig. 23 shows the comparison of measured TDT waveforms for serpentine delay line between with TGVGTs and OSGTs.

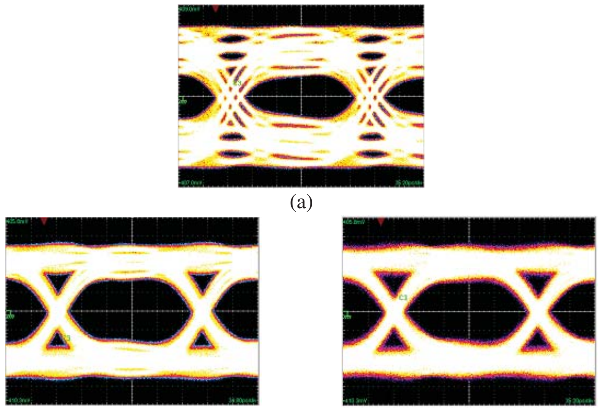

(a) (b) (c)

Fig. 25. Comparison of the measured eye diagrams for a serpentine delay line (a) without guard trace, (b) with TGVGTs, and (c) with OSGTs and a data ratio of 5 Gb/s.

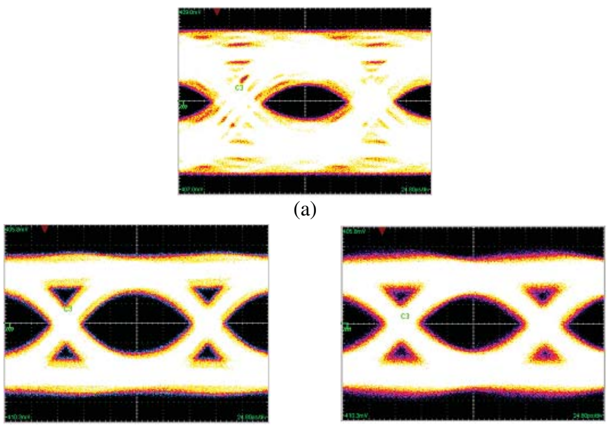

(a) (b) (c)

Fig. 26. Comparison of the measured eye diagrams for a serpentine delay line (a) without guard trace, (b) with TGVGTs, and (c) with OSGTs and a data ratio of 7.5 Gb/s.

As with the comparison of simulated results in Fig. 5, there is slight deviation in the high flat voltage level, i.e., the ringing crosstalk noise V_r, of the TDT waveform. The results of TDT waveforms for serpentine delay line with OSGTs or TGVGTs are similar except for a slight deviation. Therefore, serpentine delay line with OSGTs exhibit similar capabilities, with respect to the reduction of crosstalk, as those with TGVGTs.

The measured TDT waveforms were also compared with the simulated results in Fig. 24, for the serpentine delay line with OSGTs and without OSGTs. Fig. 24 shows that adding OSGTs reduces the maximum voltage level of the laddering wave by more than half. It is clear that the simulated TDT waveform agrees well with measurement, which validates the accuracy of the analysis.

Figs. 25 and 26 show the comparisons of the measurements for the eye diagram for a serpentine delay line with different guard traces, with data ratios of 5 Gb/s and 7.5 Gb/s, provided by a pattern generator (Anritsu MP1763C) and TDR (Tektronix CSA8000B). It is evident from Figs. 25 and 26 that, with reference to the eye diagram for the delay line without guard traces, the employment of OSGTs and TGVGTs significantly improves the eye height, eye width, and the jitter, for data ratios 5 Gb/s and 7.5 Gb/s. All of the measured values for eye diagram parameters are listed in Table V. In addition, with a data ratio 5 Gb/s, the values of eye diagram parameters, for the use of OSGTs, approach those for the use of TGVGTs. However, using OSGTs, as opposed to TGVGTs causes a small reduction in eye opening.

Although there is a slight discrepancy, the results yielded by the qualitative model, quantitative analysis, simulation, and measurement all verify the effects of crosstalk noise on the TDT waveform of a serpentine delay line and the improvement in signal integrity associated with the use of OSGTs. The improvement is more effective for cases of larger crosstalk noise, say, with more sections or smaller separation between two sections.

V. Conclusion

A guard trace is usually inserted between coupled transmission lines to reduce the crosstalk noise. Owing to the serpentine configuration, the utilization of guard traces with only two grounded vias at both ends can improve the TDT waveform and eye diagram for serpentine delay lines. However, this is not easily achieved using present manufacturing technology, because the pad of the grounded via is surrounded by a serpentine trace. This is especially true for the case of normal manufacturing technology, where the size of the via pad is larger. Therefore, using OSGTs to improve the TDT waveform and eye diagram for a serpentine delay line in embedded microstrip structure is an option recommended by the authors.

Owing to the crosstalk noise cancellation mechanism in OSGTs, the reduction in efficiency, due to crosstalk noise yielded by the use of the OSGTs is almost the same as that yielded by the use of the TGVGTs, for a serpentine delay line in the time-domain. When the amount of noise cancellation is greater the two TDT waveforms look most alike. The noise cancellation mechanism in OSGTs and ringing crosstalk noise on the TDT waveform are best illustrated by the graphic method. Two useful design graphs were constructed, the first shows TDT crosstalk noise versus the dimension for serpentine delay line with OSGTs and the second details the maximum flat voltage level of a laddering wave. The simple design guidelines for the reduction of crosstalk noise and the maintenance of good TDT waveform and eye diagrams in embedded microstrip serpentine delay line using OSGTs were also proposed.

Using the HSPICE simulation, it was demonstrated that the utilization of the OSGTs reduces the original TDT crosstalk level, thereby greatly improving eye opening and jitter. Finally, this paper also performed TDT waveform, eye diagram measurements, and 3-D full-wave simulations to validate its analyzes.

Acknowledgment

The authors would like to thank Electrical Design of Advanced Packaging and Systems Laboratory, National Taiwan University Electrical Engineering, Taipei, Taiwan.

They also commend Ansoft Corporation, Taipei, for providing the measurement equipment and simulation software.

REFERENCES

[1] R. B. Wu and F. L. Chao, "Laddering wave in serpentine delay line," *IEEE Trans. Comp. Packag. Manuf. Technol. B*, vol. 18, no. 4, pp. 644–650, Nov. 1995.

[2] W. Ruey-Beei and F.-L. Chao, "Flat spiral delay line design with minimum crosstalk penalty," *IEEE Trans. Comp. Packag. Manuf. Technol. B*, vol. 19, no. 2, pp. 397–402, May 1996.

[3] W. D. Guo, G. H. Shiue, and R. B. Wu, "Comparison between serpentine and flat spiral dealay lines on tranaient reflection/transmission waveforms and eye diagrams," *IEEE Trans. Microw. Theory Tech.*, vol. 54, no. 4, pp. 1379–1387, Jun. 2006.

[4] D. N. Ladd and G. I. Costache, "SPICE simulation used to characterize the crosstalk reduction effect of additional tracks grounded with vias on printed circuit boards," *IEEE Trans. Circuits Syst. II: Analog Digit. Singal Process.*, vol. 39, no. 6, pp. 342–347, Jun. 1992.

[5] I. Novak, B. Eged, and L. Hatvani, "Measurement by vector-network analyzer and simulation of crosstalk reduction on printed circuit boards with additional center traces," in *Proc. IEEE Instrum. Meas. Technol.*, Irvine, CA, Apr. 1993, pp. 269–274.

[6] L. Zhi, W. Qiang, and S. Changsheng, "Application of guard traces with vias in the RF PCB layout," in *Proc. IEEE Int. Symp. Electromagn. Compat.*, May 2002, pp. 771–774.

[7] A. Suntives, A. Khajooeizadeh, and R. Abhari, "Using via fences for crosstalk reduction in PCB circuits," in *Proc. IEEE Int. Symp. Electromagn. Compat.*, Aug. 2006, pp. 34–37.

[8] S. Nara and K. Koshiji, "Study of delay time characteristics of multilayered hyper-shield meander line," in *Proc. IEEE Int. Symp. Electromagn. Compat.*, Portland, OR, Aug. 2006, pp. 760–763.

[9] G. H. Shiue, C. Y. Chao, W. D. Guo, and R. B. Wu, "Improvement of time-domain transmission waveform in serpentine delay line with guard traces," in *Proc. IEEE Int. Symp. Electromagn. Compat.*, Honolulu, HI, Jul. 2007, pp. 1–5.

[10] G. H. Shiue, C. Y. Chao, and R. B. Wu, "Guard trace design for improvement on transient waveforms and eye diagrams of serpentine delay line," *IEEE Trans. Adv. Packag.*, vol. 33, no. 4, pp. 1051–1060, Nov. 2010.

[11] P. W. Chiu and G. H. Shiue, "The impact of guard trace with open stub on time-domain waveform in high-speed digital circuits," in *Proc. IEEE 18th Conf. Electr. Perform. Electron. Packag. Syst.*, Portland, OR, Oct. 2009, pp. 219–222.

[12] Y. S. Cheng, W. D. Guo, G. H. Shiue, H. H. Cheng, C. C. Wang, and R. B. Wu, "Fewest vias design for microstrip guard trace by using overlying dielectric," in *Proc. IEEE Electr. Perform. Electron. Packag.*, San Jose, CA, Oct. 2008, pp. 321–324.

[13] G. H. Shiue, J. H. Shiu, P. W. Chiu, Z. H. Zhang, M. N. Yeh, and W. C. Ku, "Improvements of time-domain transmission waveform and eye diagram of serpentine delay line using guard trace stubs in stripline structure," in *Proc. IEEE 18th Conf. Electr. Perform. Electron. Packag. Syst.*, Austin, TX, Oct. 2010, pp. 249–252.

[14] T. C. Edwards and M. B. Steer, *Foundations of Interconnect and Microstrip Design*. New York: Wiley, 2000, p. 532.

[15] C. L. Wang, G. H. Shiue, W. D. Guo, and R. B. Wu, "A systematic design to suppress wideband ground bounce noise in high-speed circuits by electromagnetic-bandgap-enhanced split powers," *IEEE Trans. Microw. Theory Tech.*, vol. 54, no. 12, pp. 4209–4217, Dec. 2006.

[16] Computer Simulation Technology. (2003). *CST Microwave Studio Manual*, Darmstadt, Germany [Online]. Available: http://www.cst.com./

[17] *Ansoft Designer. ver. 6*. Ansoft, Pittsburgh, PA [Online]. Available: http://www.ansoft.com/

[18] S. H. Hall and H. L. Heck, *Advanced Signal Integrity for High-Speed Digital System Design*. New York: Wiley, 2009, p. 680.

[19] U. S. Inan and A. S. Inan, *Engineering Electromagnetics*. New York: Wiley, 1999, p. 821.

Guang-Hwa Shiue (M'07) was born in Tainan, Taiwan. He received the M.S. degree in electrical engineering from the National Taiwan University of Science and Technology, Taipei, Taiwan, in 1997, and the Ph.D. degree in communication engineering from National Taiwan University, Taipei, in 2006.

He joined the faculty of the Department of Electronic Engineering, Chin Min Institute of Technology, Kaohsiung, Taiwan, in 1999, where he was a Lecturer. In 2001, he joined the faculty of the Department of Electronic Engineering, Jinwen University of Science and Technology, Taipei, where he was a Lecturer from 2001 to 2006, and became an Assistant Professor from 2006 to 2008. In 2008, he joined the Faculty of Electronic Engineering, Chung Yuan Christian University, Jhongli, Taiwan, where he is currently an Assistant Professor. His current research interests include numerical electromagnetic fields, microwave planar circuits, signal/power integrity for high-speed digital systems and electromagnetics interference/compatibility for high-speed/frequency electronic systems, and electrical characterization of system-in-package.

Jia-Hung Shiu was born in Changhua, Taiwan, in 1987. He received the B.S. degree in electrical engineering from Chung Yuan Christian University, Jhongli, Taiwan, in 2009. He is currently pursuing the M.S. degree in communication engineering with the same university.

His current research interests include signal integrity and electromagnetics compatibility for high-speed digital circuits.

Po-Wei Chiu was born in Miaoli, Taiwan, on June 21, 1985. He received the M.S. degree in electrical engineering from Chung Yuan Christian University, Jhongli, Taiwan, in 2010.

His current research interests include signal integrity issues in the design of high-speed digital systems.

Che-Ming Hsu was born in Taoyuan, Taiwan, in 1987. He received the B.S. degree in electrical engineering from Chung Yuan Christian University, Jhongli, Taiwan, in 2010. He is currently pursuing the M.S. degree in communication engineering with the same university.

His current research interests include signal/power integrity and electromagnetics compatibility design for high-speed digital circuits.